

# Provenance and tectonic setting of Miocene siliciclastic sediments, Sibuti formation, northwestern Borneo

R. Nagarajan · John S. Armstrong-Altrin · Franz L. Kessler ·  
Elisa L. Hidalgo-Moral · Dominique Dodge-Wan · Nur Iskandar Taib

Received: 24 May 2014 / Accepted: 6 February 2015 / Published online: 26 February 2015  
© Saudi Society for Geosciences 2015

**Abstract** Provenance and tectonic setting of sandstone and mudstone units of the Miocene Sibuti Formation from north-west Borneo have been studied based on the mineralogy, major and trace element geochemistry data. The X-ray diffraction (XRD) and scanning electron microscopy-energy dispersive spectrometry (SEM-EDS) data revealed that the sandstones and mudstones were abundant in quartz, pyrite, clay, and heavy minerals such as zircon, rutile, and some detrital cassiterite. Geochemically, the sandstones and mudstones are classified into quartz arenite, litharenite, sublitharenite, arkose, and wacke. Quartz arenites are enriched with SiO<sub>2</sub>, Zr, and

Th and depleted in Al<sub>2</sub>O<sub>3</sub>, CaO, and other elements compared to other sandstone types, indicating high maturity and intensive weathering. Chemical index of alteration (CIA: 77–90), plagioclase index of alteration (PIA: 86–100), and A-CN-K diagram suggest intense weathering in the source area. Elemental ratios such as La/Sc, Th/Sc, Cr/Th, La/Co, and Th/Co are similar to sediments derived from the felsic rocks. Also, the provenance discrimination diagrams suggest recycled continental nature of these clastic sediments which are mostly derived from metasedimentary source (Rajang Formation). Discriminant-function diagram for the tectonic discrimination of siliciclastic sediments revealed that the sediments of Sibuti Formation were derived from a collision zone, which is consistent with the geology of the study area.

**Electronic supplementary material** The online version of this article (doi:10.1007/s12517-015-1833-4) contains supplementary material, which is available to authorized users.

R. Nagarajan (✉) · D. Dodge-Wan  
Department of Applied Geology, Faculty of Engineering and  
Science, Curtin University, CDT 250, 98009 Miri, Sarawak,  
Malaysia  
e-mail: nagageochem@yahoo.com

R. Nagarajan  
e-mail: nagarajan@curtin.edu.my

J. S. Armstrong-Altrin  
Instituto de Ciencias del Mar y Limnología, Unidad de Procesos  
Oceánicos y Costeros, Universidad Nacional Autónoma de México,  
Circuito Exterior s/n, 04510 México, DF, México

F. L. Kessler  
LUNDIN Malaysia B.V, Level 13A Menara HLA, 3 JLN Kia Peng,  
Kuala Lumpur, Malaysia

E. L. Hidalgo-Moral  
Posgrado en Ciencias del Mar y Limnología, Universidad Nacional  
Autónoma de México, Circuito Exterior s/n, 04510 México, DF,  
México

N. I. Taib  
Department of Geology, Faculty of Science, University of Malaya,  
50603 Kuala Lumpur, Malaysia

**Keywords** Provenance · SEM-EDS · Miocene · Chemical weathering · Malaysia

## Introduction

Whole rock geochemistry of clastic sediments is a powerful tool to elucidate the evolution of sedimentary basins and has been widely used to reconstruct the paleoweathering, hydraulic sorting, recycling, provenance, and tectonic setting of the sedimentary basins (Abou Elmagd et al. 2014; Jorge et al. 2013; Mortazavi et al. 2014; Nagarajan et al. 2014). Behavior of elements is different during sedimentary processes, thus preserve the characteristics of source rocks. Chemical variations of clastic sediments may yield useful information about sedimentary evaluation, and thus, the relationship between source area and sedimentary basin can be extracted through geochemistry (Perri 2014). Particularly, certain elements (e.g., Th, Sc, and rare earth elements) withstand against

weathering, erosion, and transport and preserve the sedimentary record of their source (McLennan et al. 1990). When sediments are fine grained, petrography does not have their significance, and thus, any interpretation relies on geochemistry (Imchen et al. 2014). Different behavior of elements is considered in geochemistry to decipher the chemical weathering (Na and Ca are mobile elements; Nesbitt and Young 1982) and provenance. High field strength elements (HFSEs), rare earth elements (REEs), and Cr, Co, and Sc have more advantage than other elements since they are least affected by secondary processes like diagenesis and metamorphism (Cullers and Podkovyrov 2000).

Borneo is ranked as the third largest island in the world, which covers an area of 748,168 km<sup>2</sup>. It is located at the boundaries of Eurasia, Pacific Ocean, and India-Australian plates, and its motion is affected by the tectonic setting of these three plates. Borneo Island includes Indonesia (Kalimantan), East Malaysia (Sarawak and Sabah states of Malaysia), and Brunei. Particularly, NW Borneo is economically important due to richness of a world class hydrocarbon province. The geology of Sarawak consists of three distinct provinces, namely west Sarawak, central Sarawak, and north Sarawak. The north Sarawak region occupies the north and east of the Rajang–Baram watershed. During early Miocene, microcontinental fragments collided with western edge of Borneo. Vast amount of clastic sediments (~12 km thickness) were deposited in the marginal basins on and around Borneo, throughout the Neogene period (Hall and Nichols 2002). An alternative model was presented by Kessler (2009, 2010) in which the fore deep originated by crustal stretch during the Miocene and faced moderate Miocene compression, plus strike-slip movements at the Baram line that offsets the foredeep against central Luconia. Sedimentary Formations of NW Borneo mainly consist of siliciclastic sediments (sandstone, siltstone, and shale) deposited by continuous sedimentation throughout the Tertiary period. North Sarawak region is underlain by thick sequences of shallow and deep marine sediments (Liechti et al. 1960). The formations are Nyalau, Setap, Tangap (Suai), Sibuti, Belait, Lambir, Miri, and Tukai, which range in age from Oligocene to Pliocene. In north Sarawak, along the coastal regions, outcrops are formed by clastic sediments of Tukai and Miri Formations (Belait group). The youngest (Pliocene–Pleistocene) sediments are found in Brunei (Seria and Liang Formations). Though the Neogene sedimentary successions show lithological similarities over large areas, there are still some significant changes in lateral facies observed. Siliciclastic sediments of NW Borneo are described lithostratigraphically rather than by means of chronostratigraphy due to limitations of fossil record. Lithostratigraphy and tectonic setting of northern Borneo have been described by many studies; however, the tectonic setting is still being discussed by many authors (Mat-Zin and Tucker 1999; Hutchison et al. 2000; Peng et al. 2004; Hutchison 2005

(references there in); Van der Zee and Urai 2005; Morley et al. 2008; Hall et al. 2008; Kessler 2009, 2010; King et al. 2010; Hall 2013 (references there in)). Geochemical and mineralogical characters of Neogene Borneo sediments are reported in limited number of studies (Tanean et al. 1996; van Hattum et al. 2006, 2013; Nagarajan et al. 2014). However, the geochemistry of the Sibuti sediments has not been studied. In this study, the mineralogical and geochemical analyses were carried out for the clastic sediments of the Sibuti Formation, NW Borneo to infer the paleoweathering, source rock characteristics, and tectonic setting.

### Geological setting

Sibuti sediments are well exposed in the Bekenu region, and two outcrops exposed in the Ranchah-Ranchah and Tengah villages near the Bekenu town were selected for this study, which are located approximately 70 km toward SW direction from Miri (Fig. 1). The geophysical and geological evidences (Moss and Wilson 1998; van Hattum et al. 2013) suggest that throughout the Cenozoic Era, the SE Asian region was an exceptionally dynamic tectonic region. According to Hutchison (2005), the Sibuti sediments are considered as a member of Setap Formation of Miocene age. Hutchison (2005) also stated that the lithologies found were shale, with thin layer of limestone and sandstones. The Sibuti member is underlain by Suai Formation (fault contact) and overlain by Lambir Formation along a conformable but abrupt boundary (Banda 1998; Hutchison 2005). Recent work (unpublished to date) has identified muddy carbonate ramp settings with a total carbonate thickness of up to 80 m in an abandoned quarry near Kampung Opak. Based on the stratigraphic column of Sarawak, the Sibuti Formation formed between late Oligocene to early middle Miocene, and it lies between the Nyalau and Lambir Formations (Ho 1978; Fig. 2a; Liechti et al. 1960). The Setap Formation is comparable with Meligan Delta (stage III or TB 2.1–2.3; Balaguru and Lukie 2012), accumulated during mid-early Miocene. The Meligan Formation is dominated by thick sandy deltaics with subordinate sandy shallow marine facies, whereas Setap Formation consists of thin bed of sandstone within the overall shale successions, which represent that the Setap Formation is being a distal equivalent facies of the Meligan delta. The Sibuti Formation was subjected to gentle to moderate folding that led to the formation of shallow anticlinal and synclinal folds (Wannier et al. 2011). The age of the Sibuti sediments was assigned as early Miocene based on the presence of planktonic foraminifera *Globigerionoides obliquus* (Simmons et al. 1999), which is further supported by the presence of *Florschuetzia levipoli* and *Florschuetzia meridionalis*, indicating late early Miocene age. This has been further confirmed by Vermeij and Raven (2009) based on the Melongenidae sp. (*Melongenella murifactor* and *Pugilina spec.*

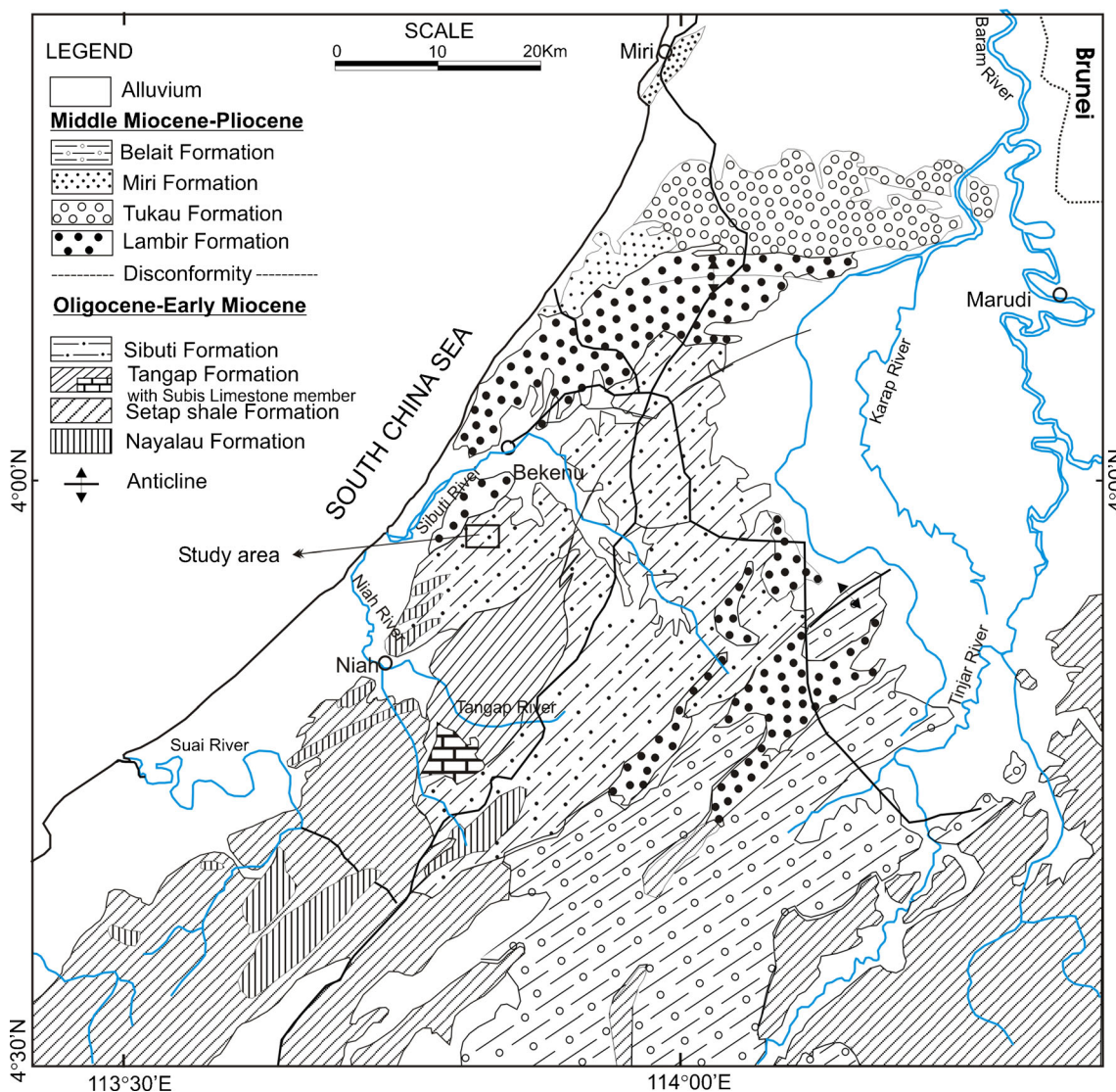


Fig. 1 Geology map of NW Borneo shows the study area (after Liechti et al. 1960)

A). The Sibuti Formation is considered as time-stratigraphically equivalent to Setap Shale Formation and termed Sibuti member of Setap Shale Formation. However, the Sibuti Formation can be distinguished from the Setap Shale Formation based on high fossil content, predominant marl lenses, and thin limestone beds (Peng et al. 2004). Based on field relationship, the Sibuti Formation could be described as a shoal surrounded by deeper shelf to slope shale deposition, ranging from marly beds, carbonate ramp deposits, and also small oyster patch reefs.

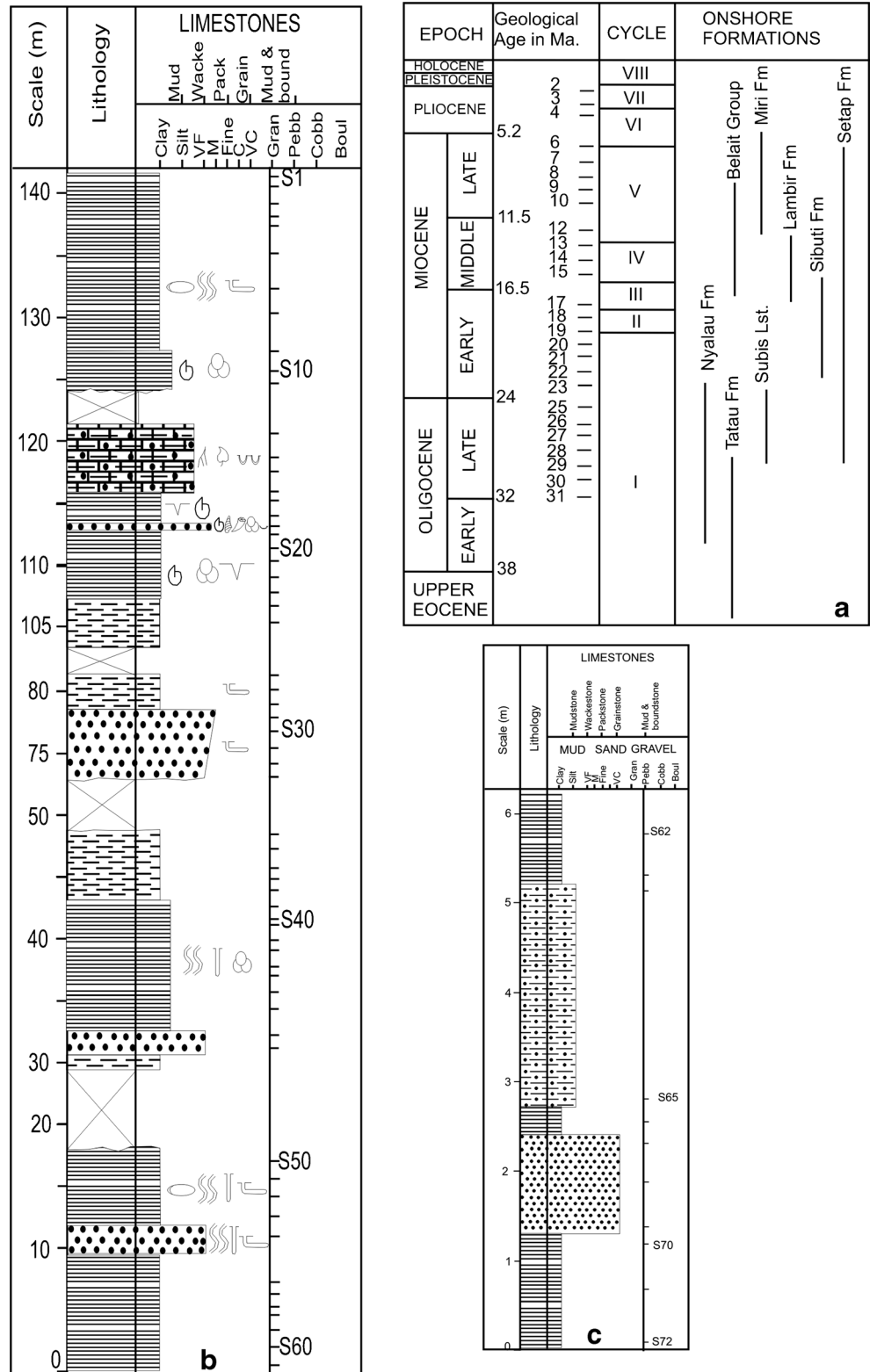
**Methodology**

In total, 73 samples were collected from two outcrops (Kampongs Ranchah-Ranchah and Tengah) of Sibuti Formation (Fig. 2b, c). Among them, 25 samples (19 from

KGRR and 6 from KGTG) were selected for geochemical analysis and 15 samples for X-ray diffraction (XRD). Samples were chosen based on their lithology, locality, and layer thickness (Fig. 2b, c). Selected samples underwent a cleaning process, and only unweathered rocks were used for analysis. All samples were then dried at the room temperature of <40°. Dried samples were crushed and grinded using agate mortar, down to a size of 75 μ.

XRD and X-ray fluorescence (XRF) analyses were performed at geology laboratory, University of Malaya (UM), Malaysia. The samples were run for loss of ignition (LOI) and then fused with a borate flux to produce a glass bead for the analysis of major oxides using XRF (PANalytical Axios<sup>mAX</sup>). For the trace element study, 3 g of powered samples and approximately 0.5 g of wax binder—Cereox<sup>TM</sup>—were grinded together for 5 min using the agate mortar to bind the powdered samples together. The mixture was then placed

**Fig. 2** **a** Stratigraphic position of Sibuti Formation compared with other onshore formations and offshore sedimentary cycles (after Ho 1978) and **b-c** Litho-log and sampling position of Kampung Ranchach Ranchah and Tengah sections



in the pellet mould, and orthoboric acid was added to the top of the samples. The mould was placed on the hydraulic press, and pressure of 4000 lb/in<sup>2</sup> was induced onto the mould to produce pressed pellets. The samples were placed into the

PANalytical Axios<sup>mAX</sup>—XRF spectrometers for analysis. Three US Geological Survey (USGS) certified reference materials were used in the present study: (1) AGV-2, (2) GSP-2, and (3) BHVO-1, and its composition were available in the

USGS website ([http://crystal.usgs.gov/geochemical\\_reference\\_standards/granodiorite.html](http://crystal.usgs.gov/geochemical_reference_standards/granodiorite.html)) as well as by Govindaraju (1994). The precision of the present study through monitoring by standards was better than  $\pm 10\%$  except Cu and Pr. Each sample was analyzed at least three times, and average values of the triplicate analysis were reported in this study. The relative errors of duplicate samples were mostly between 0 and 5%. Some samples were studied for the scanning electron microscopic (SEM) analysis at the Petrology Laboratory, Institute of Geophysics, Universidad Nacional Autónoma de México (UNAM). The study was undertaken on a Philips XL-30 SEM with a 3.5 nm of resolution, equipped with EDAX spectrometer (energy dispersive spectrometry (EDS)) system, to determine the chemical composition during SEM observations.

XRD analysis was performed using the PANalytical Empyrean X-Ray Diffractometer. Samples that were analyzed started from the Theta position of  $5^\circ$  and ending at  $70^\circ$ , at a temperature of  $25^\circ\text{C}$  and standard generator setting of 40 mA and 45 kV. The peaks were identified using its software generator.

## Results

### Mineralogy

The XRD study indicates that the clastic sediments of Sibuti member mainly consist of quartz, mica, clay minerals (illite and kaolinite and chlorite), and zeolites with little feldspar and heavy minerals (ilmenite and tourmaline). The chemical composition measured using SEM-EDS method (qualitative analysis) reveals that the clastic sediments are rich in light minerals such as quartz, pyrite (Fig. 3d) clay minerals, and heavy minerals such as zircon, rutile, or ilmenite. The concentration of these minerals is identified by the high content of Si, S, Fe, K, Zr, and Ti (Fig. 3a–d). A euhedral-shaped zircon mineral is identified (Fig. 3a). A strong Sn peak was clearly noted from a sample from Kpg. Tengah outcrop (Fig. 3c) indicates presence of detrital cassiterite, which may be recycled from the source region or derived from tin bearing granites (i.e., van Hattum et al. 2013).

### Elemental variations

Statistical summary of major, trace, and selected rare earth element concentrations are presented in Table 1. The siltstones and mudstones were geochemically classified, and the classified types are used for further discussion.

### Geochemical classification

The geochemical classification provides information on the differentiation between mature and immature sediments (Rollinson 1993). Few classification schemes have been proposed to classify the siliciclastic sedimentary rocks using major element concentrations (Pettijohn et al. 1972; Crook 1974; Blatt et al. 1980; Herron 1988). Pettijohn et al. (1972) classification was based on the graph of  $\log(\text{Na}_2\text{O}/\text{K}_2\text{O})$  versus  $\log(\text{SiO}_2/\text{Al}_2\text{O}_3)$  and is not “particularly reliable” since Na and K are prone to be mobilized during diagenesis and metamorphism (Rollinson 1993). Hence, Herron (1988) modified Pettijohn’s diagram by replacing  $\log(\text{Na}_2\text{O}/\text{K}_2\text{O})$  with  $\log(\text{Fe}_2\text{O}_3/\text{K}_2\text{O})$  on the y-axis, which rectifies the problem of alkalis. This modified diagram permits arkoses to be in the classification, and it also measures the mineral stability and mostly used in recent studies (e.g., Armstrong-Altrin et al. 2013, 2015).

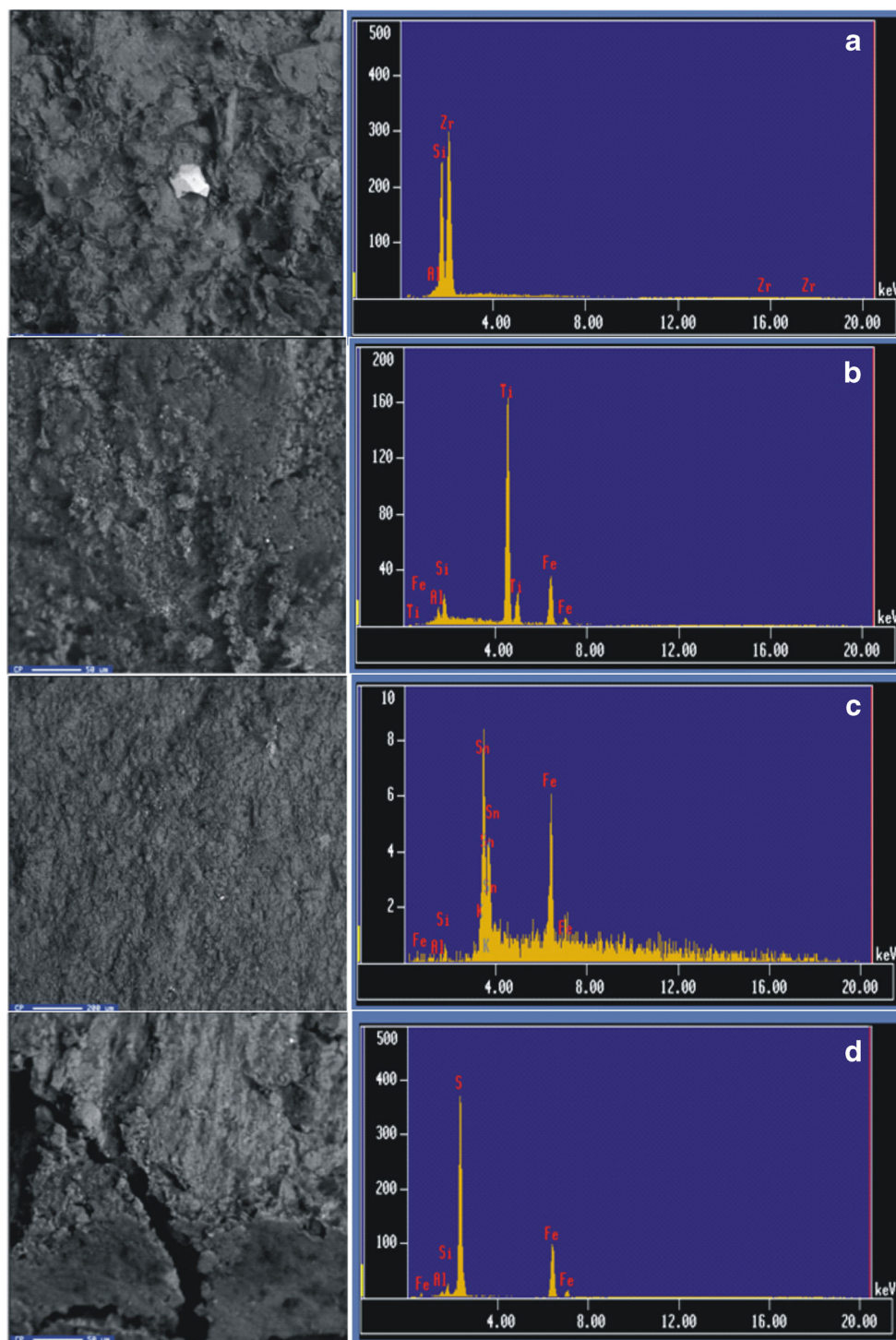
The Sibuti Formation clastic rocks were classified into quartz arenites ( $n=4$ ), litharenites ( $n=8$ ), sublitharenites ( $n=9$ ), arkoses ( $n=2$ ), subarkoses ( $n=1$ ) and wackes ( $n=2$ ) (Fig. 4; Herron 1988). For further discussion, the subarkose type is combined together with arkose type ( $n=3$ ) since it had less samples.

### Major oxides

Among major elements,  $\text{SiO}_2$  shows the largest variation, ranging from 56.2 to 96.1 wt%, which is higher in quartz arenites (87–96.1 wt%;  $91.5 \pm 4.5$ ;  $n=3$ ) than arkose (66.5–74.3 wt%;  $69.8 \pm 4.0$ ;  $n=3$ ), sublitharenite (59.5–86.2 wt%;  $68.5 \pm 7.7$ ;  $n=9$ ), litharenite (60.6–65.6 wt%;  $62.7 \pm 2.1$ ;  $n=8$ ), and wacke (56.2–56.9 wt%;  $56.6 \pm 0.6$ ;  $n=2$ ).  $\text{Al}_2\text{O}_3$  content is higher in wacke ( $19.4 \pm 0.2$ ) than in other sandstone types such as arkose ( $18.1 \pm 2.1$ ), litharenite ( $16.7 \pm 0.9$ ), sublitharenite ( $12.6 \pm 2.1$ ), and quartz arenite ( $5.9 \pm 1.9$ ). The correlation of  $\text{SiO}_2$  versus  $\text{Al}_2\text{O}_3$  ( $r=-0.90$ ),  $\text{MgO}$  ( $r=-0.92$ ),  $\text{Fe}_2\text{O}_3$  ( $r=-0.85$ ),  $\text{K}_2\text{O}$  ( $r=-0.94$ ), and  $\text{P}_2\text{O}_5$  ( $r=-0.82$ ) is statistically not significant, indicating the quartz dilution effect (Armstrong-Altrin et al. 2014). In general,  $\text{SiO}_2$  reflects the quartz content, and  $\text{Al}_2\text{O}_3$  reflects the clay mineral contents in the sediments (Jin et al. 2006), which is inversely correlated ( $r=-0.90$ ). High  $\text{SiO}_2$  and low  $\text{Al}_2\text{O}_3$  contents (i.e., quartz arenites) in the Sibuti Formation clastic sediments indicate that they are abundant in quartz and depleted in clay minerals. A statistically significant positive correlation between  $\text{Al}_2\text{O}_3$  and  $\text{K}_2\text{O}$  ( $r=0.98$ ) reveals that the K-bearing minerals have significant effect on Al distribution, which is controlled by clay minerals (Jin et al. 2006).

The concentration of  $\text{Fe}_2\text{O}_3$  and  $\text{MgO}$  are higher in wacke ( $7.6 \pm 0.8$  and  $2.4 \pm 0.01$  wt%, respectively) than in other types, decreasing in the order litharenites > sublitharenites > arkoses > quartz arenites and displayed a statistically significant positive

**Fig. 3** a–d SEM and EDS spectrum for the mudstone and sandstone samples.



correlation ( $r=0.98$ ). The average  $K_2O$  content showed minimum variation amongst all the sandstones, and the lowest value is recorded in quartz arenites ( $0.7\pm 0.2$ ). The concentrations of  $MnO$  ( $0.0$ – $0.2$  wt%),  $Na_2O$  ( $0.0$ – $0.8$  wt%),  $CaO$  ( $0.0$ – $5.5$  wt%), and  $P_2O_5$  ( $0.0$ – $0.1$  wt%) are low.  $TiO_2$  showed minimum variation, which range between  $0.4$  and  $1.4$  wt%. The low contents of  $CaO$  and  $Na_2O$  indicate that these elements were leached during intensive weathering processes.

However, sublitharenite shows the highest  $CaO$  content among other types, which is due to abundant shell and coral fragments. Quartz arenites show the highest  $TiO_2$  concentration ( $0.44$ – $1.40$ ), and the overall average content of  $TiO_2$  ( $0.91\pm 0.5$ ) is comparable with post-Archaean Australian shale (PAAS; Taylor and McLennan 1985).  $TiO_2$  is negatively correlated with  $Al_2O_3$  suggesting that  $TiO_2$  is not associated with phyllosilicate minerals especially with illite (Dabard

**Table 1** Statistical summary (range, mean, and standard deviation) of geochemical data of classic sediments of the Sibuti Formation

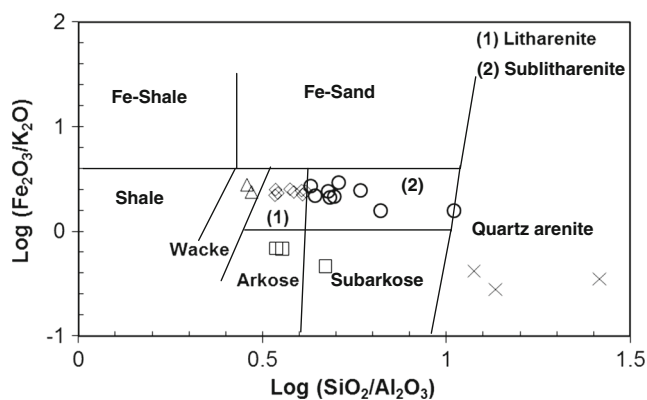
Rock name	Wacke (n=2)	Quartz arenite (n=3)	Arkose (n=3)	Litharenite (n=8)	Sublitharenite(n=9)	PAAS <sup>a</sup>	UCC <sup>b</sup>
SiO <sub>2</sub>	56.03–56.91; 56.5±0.6	87.4–93.9; 90.1±3.4	65.13–71.97; 67.6±3.8	60.39–64.66; 62.5±1.9	59.42–83.18; 67.7±6.8	62.40	66.00
TiO <sub>2</sub>	0.81–0.82; 0.81±0.01	0.44–1.40; 0.91±0.5	0.78–0.86; 0.81±0.04	0.76–0.83; 0.79±0.03	0.52–0.91; 0.69±0.1	0.99	0.50
Al <sub>2</sub> O <sub>3</sub>	19.27–19.54; 19.4±0.2	3.60–7.36; 5.8±2	15.33–18.89; 17.5±1.9	15.58–17.65; 16.6±0.8	7.94–15.17; 12.5±2.2	18.78	15.20
Fe <sub>2</sub> O <sub>3</sub>	7.02–8.13; 7.6±0.8	0.17–0.37; 0.25±0.1	1.06–1.78; 1.5±0.4	5.48–6.55; 6.0±0.3	2.14–5.78; 4.6±1.3	7.18	4.50
MgO	2.35–2.36; 2.4±0.01	0.08–0.23; 0.17±0.1	0.62–1.03; 0.88±0.2	1.84–2.21; 2±0.1	0.54–1.83; 1.5±0.4	2.19	2.20
CaO	0.25–0.39; 0.32±0.1	0.01–0.02; 0.009±0.006	0.00–0.04; 0.02±0.02	0.14–0.91; 0.43±0.2	0.04–5.50; 2.7±2	1.29	4.20
Na <sub>2</sub> O	0.39–0.41; 0.4±0.02	–	0.03–0.32; 0.18±0.1	0.23–0.63; 0.46±0.1	0.48–0.80; 0.66±0.1	1.19	3.90
K <sub>2</sub> O	2.93–2.97; 2.9±0.03	0.49–0.88; 0.70±0.2	2.29–2.61; 2.5±0.2	2.40–2.76; 2.56±0.1	1.37–2.34; 2.0±0.3	3.68	3.40
P <sub>2</sub> O <sub>5</sub>	0.08–0.10; 0.094±0.01	0.01–0.04; 0.023±0.02	0.04–0.05; 0.05±0.01	0.06–0.09; 0.067±0.01	0.03–0.09; 0.065±0.02	0.16	0.17
LOI	9.26–9.82; 9.5±0.4	1.45–2.89; 2.1±0.7	7.86–9.56; 9.0±1.0	7.50–9.68; 8.4±0.8	3.09–10.18; 7.5±2.2	–	–
SiO <sub>2</sub> /Al <sub>2</sub> O <sub>3</sub>	2.87–2.95; 2.9±0.06	11.87–26.08; 17.2±7.8	3.45–4.69; 3.9±0.7	3.42–4.15; 3.8±0.3	4.27–10.48; 5.7±1.9	3.32	4.34
K <sub>2</sub> O/Na <sub>2</sub> O	7.09–7.56; 7.3±0.3	–	7.85–67.40; 29.6±32.8	3.90–11.90; 6.1±2.5	1.78–4.59; 3.2±0.8	3.09	0.87
K <sub>2</sub> O/Al <sub>2</sub> O <sub>3</sub>	0.15	0.11–0.14; 0.12±0.01	0.13–0.15; 0.14±0.01	0.15–0.16; 0.15	0.15–0.17; 0.16±0.01	0.20	0.22
Al <sub>2</sub> O <sub>3</sub> /TiO <sub>2</sub>	23.84–23.91; 23.9±0.05	4.66–8.28; 7.1±2.1	19.33–24.13; 21.6±2.4	19.89–22.52; 21.0±0.9	8.69–22.19; 18.5±3.9	18.97	30.40
CIA	84.00	88.00–90.00; 89±1	87.00	82.00–85.00; 83.0±1.1	77.00–81.00; 79.1±1.5	–	–
PIA	95.00–96.00; 95.5±0.7	100.00	98.00–100.00; 99.0±1.0	93.00–98.00; 94.5±1.7	86.00–92.00; 89.2±1.9	–	–
ICV	0.72–0.77; 0.74±0.04	0.29–0.39; 0.33±0.05	0.31–0.35; 0.33±0.02	0.70–0.77; 0.74±0.02	0.73–1.33; 1±0.2	–	–
Sc	22.67–23.01; 22.8±0.24	–	12.04–13.13; 12.6±0.6	15.29–20.25; 18±1.8	0.03–14.93; 10.8±5	16.00	11.00
V	144.89–145.16; 145.0±0.2	31.56–75.05; 58.3±23.4	96.16–117.50; 110.4±12.3	116.66–140.90; 128.5±9.1	51.30–108.45; 88.7±18.7	150.00	60.00
Cr	117.58–121.37; 119.5±2.7	28.85–205.66; 102.6±92	85.12–93.31; 89.7±4.2	93.79–108.70; 101.8±4.8	45.92–119.51; 82.6±19.1	110.00	35.00
Mn	475.60–1186.84; 831.2±502.9	–	6.33–13.27; 6.5±4.9	397.36–1004.83; 577.4±225.1	23.87–1503.91; 627.5±437.2	852.00	600.00
Co	26.50–29.11; 27.8±1.8	–	1.00	18.44–24.10; 21.4±1.9	1.65–17.03; 11.9±4.9	23.00	10.00
Ni	66.47–81.14; 73.8±10.4	30.83–37.95; 34.0±3.6	68.42–91.93; 82.4±12.4	62.54–128.50; 78.4±21.1	39.32–72.93; 59.2±9.8	55.00	20.00
Cu	56.52–63.24; 59.9±4.8	59.19–97.98; 75.1±20.3	73.99–212.49; 121.3±79	50.95–66.99; 60.3±6.1	40.59–60.70; 49.0±6.3	50.00	25.00
Zn	133.97–149.98; 142.0±11.3	72.59–81.91; 75.7±5.3	97.93–145.60; 121.1±23.9	127.02–169.11; 136.2±13.7	90.48–123.57; 107.7±9.7	85.00	71.00
Rb	161.36–176.68; 169.0±10.8	82.64–103.87; 93.8±10.6	184.04–204.56; 195.7±10.5	149.21–170.80; 156.8±8	109.80–146.28; 126.6±12.3	160.00	112.00
Sr	201.70–209.86; 205.8±5.8	156.57–172.13; 165.1±7.9	195.03–211.99; 202.5±8.6	175.15–210.68; 193.1±12.1	198.58–328.18; 252.5±42.1	200.00	350.00
Y	24.79–25.99; 25.4±0.8	25.35–40.08; 32.0±7.5	31.68–34.16; 32.5±1.4	25.11–26.38; 25.6±0.4	22.71–31.65; 25.0±2.6	27.00	22.00
Zr	179.42–194.74; 187.1±10.8	436.51–553.173; 2558.8	284.49–536.63; 374.0±141.1	211.03–336.69; 246.7±41	255.25–2245.38; 575.6	210.00	190.00
Nb	18.01–22.97; 20.5±3.5	39.96–56.26; 47.1±8.3	37.38–43.58; 39.8±3.3	21.94–23.92; 23.6±0.7	18.62–40.95; 25.7±7.1	19.00	25.00
Mo	0.00–5.18; 2.59±3.7	98.02–266.70; 165.7±89.1	59.04–101.3; 75.6±22.6	0.00–12.49; 6.1±3.7	0.00–131.69; 31.3±45.5	–	1.50
Ba	597.65–752.75; 675.2±109.7	337.95–860.88; 605.9±261.7	934.99–1145.01; 1047.7±105.9	710.20–807.38; 765.7±34	545.28–1135.60; 796.9±173.8	650.00	550.00
La	124.52–174.38; 149.5±35.3	74.11–231.72; 152±78.8	219.46–290.23; 258.6±36.0	161.55–193.13; 175.5±11.2	113.90–300.17; 192.1±56.5	38.00	30.00
Ce	252.82–334.52; 293.7±57.8	143.24–431.39; 284.5±144.2	462.05–572.29; 521.3±55.6	315.29–382.35; 348.7±23.5	221.02–577.92; 378.1±110.1	80.00	64.00
Pr	27.33–33.45; 30.4±4.3	14.44–41.54; 27.9±13.6	40.10–50.50; 46.2±5.5	31.70–38.64; 35.7±2.2	25.61–52.80; 37.8±8.4	7.83	7.10

Table 1 (continued)

Rock name	Wacke ( $n=2$ )	Quartz arenite ( $n=3$ )	Arkose ( $n=3$ )	Litharenite ( $n=8$ )	Sublitharenite ( $n=9$ )	PAAS <sup>a</sup>	UCC <sup>b</sup>
Nd	126.67–160.27; 143.5±23.8	28.92–212.84; 120.0±92	214.19–281.6; 254.1±35.4	148.61–204.54; 183.6±17.5	109.68–293.68; 197.0±57.6	32.00	26.00
Sm	20.13–22.09; 21.1±1.4	8.88–27.06; 17.8±9.1	26.51–32.67; 30.3±3.3	20.71–27.10; 25.1±2	18.33–34.00; 26.3±5.1	5.60	4.50
Hf	7.59–9.53; 8.6±1.4	21.26–100.34; 52.3±42.2	16.36–21.99; 18.6±3.0	9.50–11.99; 10.8±0.7	9.65–42.05; 15.3±10.2	5.00	5.80
Pb	44.24–47.48; 45.9±2.3	48.48–54.48; 52.0±3.1	57.14–61.93; 59.4±2.4	42.62–50.26; 46.5±2.7	35.06–56.41; 43.6±7	20.00	20.00
Th	36.30–43.66; 40.0±5.2	82.60–101.10; 89.5±10.1	74.85–83.94; 78.4±4.8	43.30–47.69; 46.4±1.4	37.10–76.59; 49.2±11.6	14.60	10.70
U	2.09–2.20; 2.1±0.08	2.75–2.87; 2.8±0.07	2.61–2.78; 2.7±0.09	2.20–2.27; 2.2±0.02	2.15–2.66; 2.3±0.2	3.10	2.80
La/Sc	5.49–7.58; 6.5±1.5	–	16.71–24.10; 20.6±3.7	8.02–11.88; 9.9±1.4	7.63–9756.48; 1099.5	2.38	2.73
Th/Sc	1.60–1.90; 1.7±0.2	–	5.70–6.97; 6.2±0.7	2.25–3.07; 2.6±0.3	2.49–3063.40; 344.2	0.91	0.97
La/Th	3.43–3.99; 3.7±0.4	0.73–2.81; 1.8±1	2.93–3.48; 3.3±0.3	3.57–4.05; 3.8±0.2	3.06–5.71; 3.9±0.9	2.60	2.80
Zr/Hf	20.44–23.65; 22.0±2.3	20.53–55.13; 41.4±18.4	17.18–24.40; 19.7±4.1	19.84–28.08; 22.7±2.6	22.92–53.40; 33.3±11.2	42.00	32.76
Cr/Ni	1.50–1.77; 1.6±0.2	0.76–6.67; 3.2±3.1	1.05–1.24; 1.1±0.1	0.85–1.51; 1.4±0.2	0.81–1.93; 1.4±0.4	2.00	1.75
Cr/Th	2.78–3.24; 3.0±0.3	0.35–2.03; 1.08±0.9	1.01–1.25; 1.2±0.1	2.02–2.41; 2.2±0.1	0.92–2.14; 1.7±0.4	7.53	3.27
Th/Co	1.25–1.65; 1.4±0.3	–	0–74.93; 37.5±43.3	1.80–2.52; 2.2±0.2	2.46–30.26; 5.7±9.6	0.63	1.07
Th/Cr	0.31–0.36; 0.33±0.04	0.49–2.86; 1.50±1.2	0.80–0.99; 0.9±0.1	0.41–0.50; 0.5±0.03	0.47–1.09; 0.62±0.2	0.13	0.31
Rb/Sr	0.77–0.88; 0.82±0.08	0.53–0.62; 0.57±0.05	0.87–1.02; 1.0±0.09	0.71–0.98; 0.8±0.08	0.36–0.67; 0.52±0.1	0.80	0.32
Th/U	17.40–19.82; 18.6±1.7	30.00–35.20; 32.0±2.8	28.68–30.18; 29.3±0.8	19.65–21.11; 20.7±0.5	17.21–28.77; 21.1±3.4	4.71	3.82
Zr/Sc	7.91–8.46; 8.2±0.4	–	21.67–44.56; 30.0±12.7	10.81–20.71; 14.0±3.3	20.68–89815.32; 10,008.1	13.13	17.27
Sc/Th	0.53–0.62; 0.58±0.07	–	0.14–0.18; 0.16±0.02	0.33–0.44; 0.4±0.04	0.0–0.40; 0.24±0.1	1.10	1.03
Co/Th	0.61–0.80; 0.70±0.1	–	0–0.01; 0.007±0.01	0.40–0.56; 0.46±0.05	0.0–0.41; 0.27±0.2	1.58	0.93
(La/Sm)/N	3.89–4.97; 4.43±0.8	5.26–5.41; 5.35±0.09	5.21–5.59; 5.4±0.2	4.17–4.94; 4.4±0.2	3.91–5.56; 4.5±0.5	4.33	–

<sup>a</sup> Post-Archean Australian Shale (Taylor and McLennan 1985); <sup>b</sup> Upper Continental Crust (McLennan 2001)





**Fig. 4** Classification of sandstones using  $\log (\text{SiO}_2/\text{Al}_2\text{O}_3)$ – $\log (\text{Fe}_2\text{O}_3^*/\text{K}_2\text{O})$  diagram (after Herron 1988)

1990). The titanium oxides may occur as either poorly crystalline masses, cryptocrystalline aggregates, or discrete, euhedral crystals of anatase, ilmenite, brookite, and rutile that attain a variety of crystal habits.  $\text{TiO}_2$  does not show any relationship with any major elements which indicates that it is not associated with either phyllosilicates or ilmenite. Thus, the high content of  $\text{TiO}_2$  in quartz arenites should be due to the presence of heavy mineral rutile which has been clearly identified in the SEM-EDS study (Fig. 3b).

Major elements were normalized against average UCC values (Taylor and McLennan 1985; McLennan 2001) and shown in Fig. 5a. Quartz arenites show enrichment in  $\text{SiO}_2$  and  $\text{TiO}_2$  and depletion in other major elements compared to other rock types as well as to UCC. All the samples except for quartz arenites and sublitharenites show enrichment in  $\text{Al}_2\text{O}_3$  content. Wackes, litharenites, and sublitharenites are enriched in  $\text{Fe}_2\text{O}_3$ , and  $\text{Na}_2\text{O}$ ,  $\text{K}_2\text{O}$ ,  $\text{P}_2\text{O}_5$ , and  $\text{CaO}$  are depleted when compared with UCC.

#### Trace element concentrations

Table 1 shows the minimum, maximum, average, and standard deviation for the trace element concentrations of rock samples from the Sibuti Formation.

#### Large ion lithophile elements (LILEs)

Rb content varies from 93.8 to 195.7 ppm. The lowest concentration of Rb is in quartz arenite ( $93.8 \pm 10.6$ ) whereas the highest concentration is in arkoses ( $195.7 \pm 10.5$ ). Rb is positively correlated with  $\text{Al}_2\text{O}_3$  and  $\text{K}_2\text{O}$  contents. The high abundance of Rb suggests that the sediments also consist of very fine-grained clays and silts (Kessler and Nagarajan 2012). The lowest concentration of Sr is shown by quartz arenites ( $165.1 \pm 7.9$ ), and the highest concentration is shown by sublitharenites ( $252.5 \pm 42.1$ ). Ba has a wide variation among different types of sandstones (~606–1048 ppm). The lowest and highest concentrations of Ba are recorded in quartz

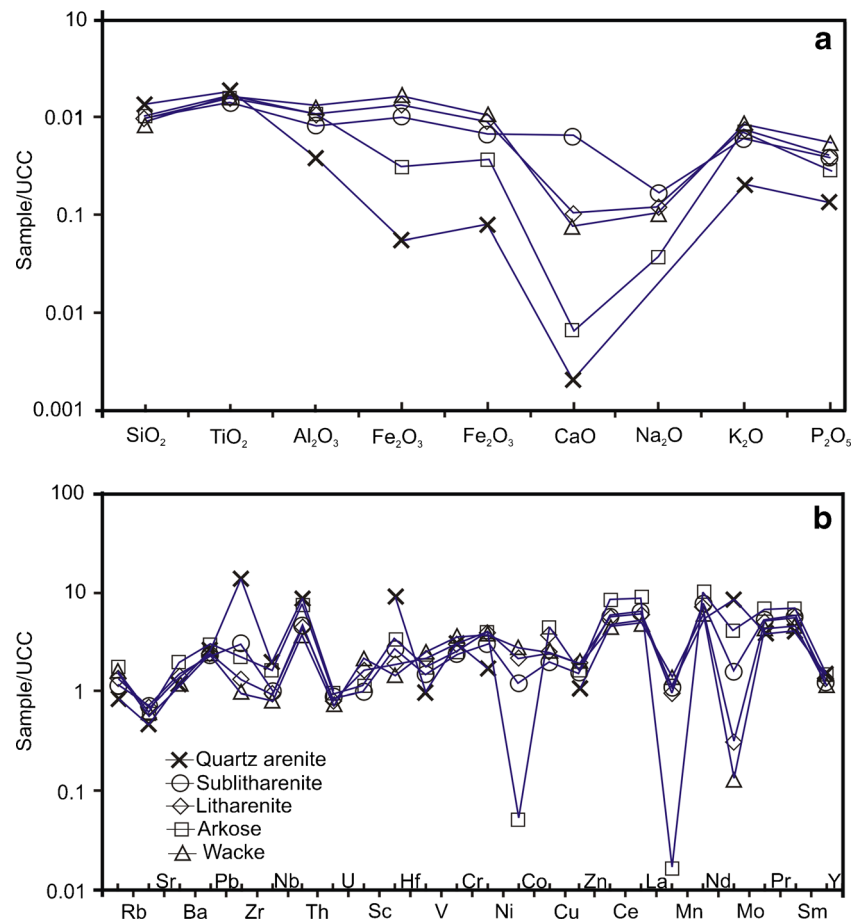
arenites ( $606 \pm 262$ ) and arkoses ( $1048 \pm 106$ ), respectively. The proportion of clay minerals in different rock types could be the reason explaining the variations in Ba content. Compared to UCC, Rb and Ba contents are enriched and Sr content is depleted (Fig. 5b). Overall, Rb, Ba, and Sr recorded low concentrations in quartz arenites and high in arkoses (Fig. 5b). Sr and Ba usually reside in plagioclase and K-feldspar, respectively (Puchett 1972). But, Ba does not show any significant correlation with  $\text{K}_2\text{O}$ ,  $\text{Al}_2\text{O}_3$ , and Rb indicating that Ba is not mainly associated with feldspars (Nagarajan et al. 2007b). Sr shows a strong positive correlation with CaO ( $r=0.94$ ) and moderate correlation with  $\text{Na}_2\text{O}$ , and MnO ( $r=0.54$ ,  $0.57$ , respectively) indicates that Sr is mainly associated with carbonates and minor amount with Na-feldspar (albite).

#### Ferromagnesian trace elements

The Cr content is higher in wacke ( $119.5 \pm 2.7$ ) than in quartz arenites ( $102.6 \pm 92$ ), litharenites ( $101.8 \pm 4.8$ ), arkoses ( $89.7 \pm 4.2$ ), and sublitharenites ( $82.6 \pm 19.1$ ). The Ni content is higher in arkoses ( $82.4 \pm 12.4$ ) than in litharenites ( $78.4 \pm 21.1$ ), wackes ( $73.8 \pm 10.4$ ), sublitharenites ( $59.2 \pm 9.8$ ), and quartz arenites ( $34.0 \pm 3.6$ ). Litharenites show wide variation of Ni content which ranges from 62.54 to 128.50 ppm. On the other hand, the concentration of V is high in wackes ( $145.0 \pm 0.2$ ) while the lowest is shown by quartz arenites ( $58.3 \pm 23.4$ ). According to Cox and Lowe (1995) and Armstrong-Altrin et al. (2004), the presence of mica may control the distribution of Cr and V. In this study, Cr, Ni, and V contents are recorded higher than UCC, except V content in quartz arenites, which is lower than in other types and UCC (Fig. 5b). Scandium concentration is higher in wackes ( $22.8 \pm 0.24$ ) than arkoses ( $12.6 \pm 0.6$ ), litharenites ( $18 \pm 1.8$ ), and sublitharenites ( $10.8 \pm 5$ ). The average value of Sc in sublitharenites and arkoses are comparable with UCC while other rock types show higher content of Sc than UCC. Cobalt concentrations in wackes, litharenites, and sublitharenites range from 29.11 to 26.50 ppm, 18.44 to 24.10 ppm, and 1.65 to 17.03 ppm, respectively, and arkoses show significant depletion in the concentration of Co, compared with UCC (Fig. 5b). Ferromagnesian trace elements such as Cr, Ni, V, Co, and Sc in the studied sandstones have no significant interrelationships, indicating the heterogeneity in the sediment source. However, Co and Sc show a significant relationship with V and  $\text{Al}_2\text{O}_3$  indicating that Co and Sc in Sibuti sediments is partly controlled by chlorite and other accessory non-aluminous silicate minerals (Rahman and Suzuki 2007).

High-field strength elements such as Y, Zr, Nb, Th, and Hf in sedimentary rocks can provide information about the source rocks (McLennan et al. 1990; Nagarajan et al. 2007a; 2007b, 2014; Armstrong-Altrin et al. 2013) since they have minimum effects on metamorphism and weathering. Quartz arenites

**Fig. 5** Multi-element (a major b trace and REE) normalized diagram for the Sibuti sandstones, normalized against average upper continental crust values (UCC; Taylor and McLennan 1985; McLennan 2001)



show highest concentration of Zr ( $2559 \pm 2652$ ) when compared to wackes, arkoses, litharenites, and sublitharenites. Large variation in Zr concentration is shown by sublitharenites (255–2245 ppm) while other rock types recorded medium to low variations. The high concentration of Zr in quartz arenites and litharenites suggest the occurrence of heavy minerals like zircon probably derived from felsic dominated/recycled source region (Fig. 5b). Higher Zr and Hf concentrations are due to the presence of heavy minerals in the sediments, such as zircon ( $\text{ZrSiO}_4$ ), ilmenite ( $\text{TiO}_2$ , FeO,  $\text{Fe}_2\text{O}_3$ ), or rutile ( $\text{TiO}_2$ ). Occurrence of zircon in the studied sediments is confirmed by SEM-EDS analysis (Fig. 3a) and by linear positive correlation between Zr and Hf ( $r=0.98$ ). In particular, high content of Zr in quartz arenites may be due to sorting effect of sediments during transportation.

Niobium (Nb) concentration could give an indication of provenance in geochemical study of clastic rocks (Condie 1993; Skilbeck and Cawood 1994). Most of the samples show quite high concentration of Nb ranging from 20.5 to 47.1 ppm. Quartz arenites show the highest concentration of Nb (avg.  $47.1 \pm 8.3$ ) while the lowest concentration is shown by wackes ( $20.5 \pm 3.5$  ppm). When comparing with PAAS and UCC, Nb shows slight enrichment in all the samples. High

concentration of Nb in Sibuti Formation could indicate that there is a significant fractionation of Nb from the source rocks (Hofmann 1988). Besides that, quartz arenites also show the highest concentration of Th with an average of  $89.5 \pm 10.1$  and ranging from 82.60 to 101.10 ppm. On the other hand, the lowest concentration is recorded by wackes ( $40.0 \pm 5.2$  ppm). Large variation of Th is shown by sublitharenites, ranging between 37 and 77 ppm. The concentration of Th is higher than in PAAS and UCC values. Nb, Th, Zr, Ti, Cr, and Hf contents are enriched in quartz arenites, and a strong positive relationship amongst these elements clearly indicates that these elements are associated with heavy minerals, which are common in quartz arenites, and these elements survived against intensive weathering in the source area and transported from the source region.

## Discussion

### Paleoweathering

Chemical weathering progressively modify the original mineralogy of basement crystalline rocks, by changing into clays, secondary oxides, and hydrous minerals (Nesbitt et al. 1997).

Mineral maturity of sediments mainly reflects the weathering process, where the degree of conversion of feldspar to aluminous clays is related to intensity of paleoweathering, paleoclimate, and tectonism (Fedo et al. 1996; Nesbitt et al. 1997; Hurowitz and McLennan 2005; Armstrong-Altrin et al. 2013; Nagarajan et al. 2014). The degree of weathering influenced by several factors such as time and weathering intensity from physical, chemical, or both. In this study, A-CN-K ternary diagram, chemical index of alteration (CIA), plagioclase index of alteration (PIA) established by Nesbitt and Young (1982, 1984), Th/U, and Rb/Sr ratios are used to comprehend the intensity of paleoweathering in the source region.

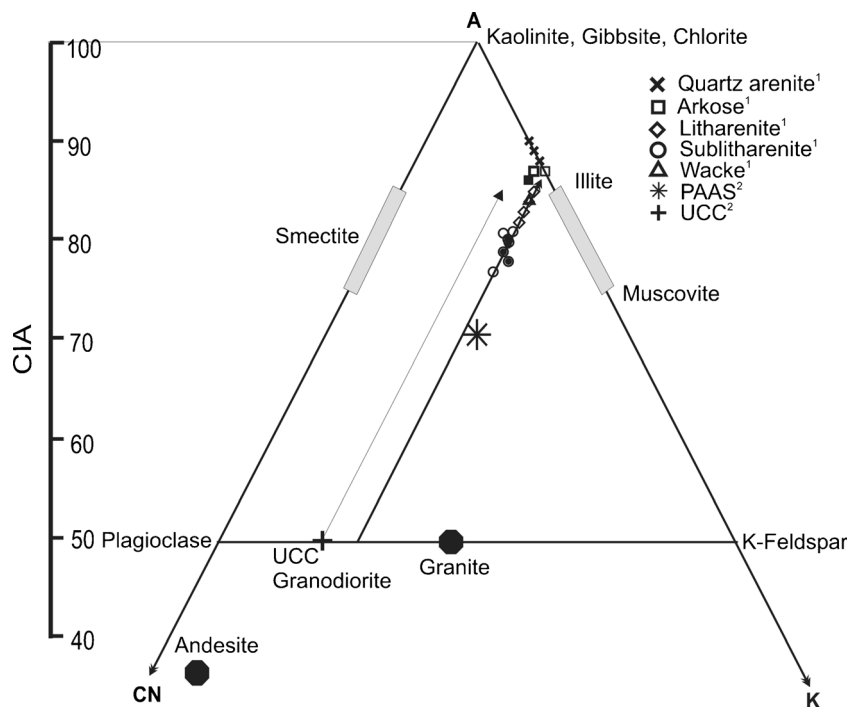
A-CN-K diagram illustrates the mobility of elements during the chemical weathering phases of source area and post-depositional chemical modifications (Nesbitt and Young 1982, 1984) particularly the loss of Ca, Na, and Sr that is proportional to the intensity of weathering (Nyakairu and Koeberl 2001; Nesbitt et al. 1997). In the A-CN-K plot (Fig. 6), individual samples plot away from the plagioclase-K-feldspar join line, UCC, and PAAS indicating moderate to intense chemical weathering in the source area. All the samples are plotted parallel to the A-CN line, and the normal weathering is oriented toward illite indicating the presence of more illite than kaolinite and smectite which is confirmed by XRD study. Samples plotted toward illite are interpreted to be the effect of potassium metasomatism, where post-depositional processes converts kaolinite to illite; however, there is no conversion trend observed toward K<sub>2</sub>O. From the ternary diagram, the samples mostly plotted between average granite and UCC line (i.e., granodiorite), suggesting the

protolith of the area to be of intermediate to felsic source rocks.

The intensity and duration of weathering in clastic sediments can also be evaluated by studying the relationship between alkali and alkaline earth elements using the indices CIA and PIA (Nesbitt and Young 1982, 1984). The CIA can be calculated using the formula (molecular proportion):  $CIA = [(Al_2O_3 / (Al_2O_3 + CaO^* + Na_2O + K_2O)) \times 100]$ , where CaO\* is the amount of CaO incorporated in the silicate fraction of the rock. The correction of CaO is done as carbonate contributions were not analyzed in this present study due to the absence of CO<sub>2</sub> value. Thus, Bock et al. (1998) assumption was adopted in the regard that CaO values were accepted only if  $CaO < Na_2O$ ; subsequently, when  $CaO > Na_2O$ , it was assumed that the concentration of CaO equals to Na<sub>2</sub>O. CIA is a suitable measure for paleoweathering as it monitors the progressive weathering conditions of feldspars to clay minerals (Fedo et al. 1995; Armstrong-Altrin et al. 2004). High and low CIA values (>76 and <50) signify intensive chemical weathering and unweathered condition at the source areas. The average values of this study show a wide variation (Table 1), i.e., as wackes (84), quartz arenites (89±1), litharenites (83±1.1), sublitharenites (79.1±1.5), and arkoses (87), which clearly signify that the source area has been subjected to moderate to intensive chemical weathering. Similarly, the average CIA values are higher than UCC value, which indicate high weathering intensity in the source region.

The PIA was calculated using the formula:  $PIA = [(Al_2O_3 - K_2O) / (Al_2O_3 + CaO^* + Na_2O - K_2O)] \times 100$ . PIA would provide quantitative estimation of secondary aluminous clay

**Fig. 6** A-CN-K ternary diagram shows the weathering trend for the sandstones of Sibuti Formation



mineral from primary feldspars (Nesbitt and Young 1982) and volcanic glasses (Fedó et al. 1995). During weathering of feldspar from the source rock, Ca is considerably leached quickly in comparison to Na and K. Therefore, with increasing intensity of weathering, the total alkali content in the rock ( $K_2O+Na_2O$ ) and ratio of  $K_2O$  and  $Na_2O$  would be inversely related, where decrease in total alkali content meant an increase in the ratio of  $K_2O/Na_2O$ . The reason being that breaking down and removal of plagioclase feldspar is preferred instead of K-feldspars (Nesbitt and Young 1984). In the present study, PIA values vary from 86 to 100. PIA value for wackes ( $95.5\pm 0.7$ ), quartz arenites (100), arkoses ( $99\pm 1.0$ ), litharenite ( $94.5\pm 1.7$ ), and sublitharenite ( $89.2\pm 1.9$ ) are higher than in UCC. High values of CIA ( $>77$ ) and PIA ( $>86$ ) suggests that the clastic sediments were subjected to intense chemical weathering.

The ratios of Th/U in sedimentary rocks are of profound interests, as this ratio reflects the weathering profile and the recycling of the sediments resulted from the loss of U (e.g., Bakkiaraj et al. 2010; Rahman and Suzuki 2007). It would also exhibit weathering intensity from the oxidation result of insoluble  $U^{4+}$  to soluble  $U^{6+}$  with the loss of solution and increase of Th/U ratios (McLennan and Taylor 1991). In addition, Th/U ratio is also useful to infer the probable source of the clastic sedimentary rocks (Bakkiaraj et al. 2010). In sedimentary rocks, Th/U ratios that are greater than or equal to four would be characterized as sedimentary rocks originating from the upper crust or sediment recycling. On the other hand, Th/U ratios lower than four would be characterized as magmatic source contributions (Roddaz et al. 2006). The average Th/U ratio in quartz arenites ( $32.0\pm 2.8$ ) is higher than in arkoses ( $28.8\pm 0.2$ ), sublitharenites ( $21.1\pm 3.4$ ), litharenites ( $20.7\pm 0.5$ ), and wackes ( $18.6\pm 1.7$ ). The high Th/U ratio ( $>4$ ) reveals that the studied clastic rocks were originated from the upper crust or recycled sediments. In addition, high Th/U ratios also signify the removal of U during intensive weathering ( $CIA>75$ ) (McLennan et al. 1980).

#### Hydraulic sorting

Geochemistry of sedimentary rocks can be influenced by hydraulic sorting, which may control the distribution of some trace elements (Armstrong-Altrin et al. 2012, 2014). Zr is mostly concentrated in zircon, while Sc is concentrated in mafic components. Zr/Sc ratio can be used as a tracer for zircon (heavy mineral concentration), and zircon enrichment in sediments can be studied by relationships between Th/Sc and Zr/Sc (McLennan et al. 1993). Th/Sc ratios show overall positive correlation with Zr/Sc for first-cycle sediments, depending on the nature of the source rocks, whereas Zr/Sc ratios show considerable variation with little accompanying change in Th/Sc ratios in mature or recycled sediments (McLennan et al. 1993).

The scatter plot of Th/Sc versus Zr/Sc (after McLennan et al. 1993) is used to distinguish the contrasting effects between the source composition and sedimentary processes on the composition of clastic sedimentary rocks. On the Th/Sc versus Zr/Sc scatter plot (Fig. 7), samples from the Sibuti Formation mostly follow the trend 2 (Fig. 7). Sublitharenites and arkoses clearly show the enrichment of zircon by sedimentary sorting or recycling. However, wackes and some litharenites follow trend 1 and indicating the nature of provenance. They follow the normal weathering trend and shows positive correlation ( $r=0.63$ ), which indicates that the samples follow the normal igneous differentiation trend and does not show zircon enrichment. The highest Th/Sc and Zr/Sc values are shown by sublitharenite. The Th/Sc ratios of the samples range from 1.60 to 9.68, whereas the ratio of Zr/Sc ranges from 7.91 to 52.6. The sample number SL25 (sublitharenite) is not included in the diagram (Fig. 7) due to its high ratio values of Th/Sc and Zr/Sc. The remaining samples follow trend 2, where sediments include concentration zircon during sedimentary sorting and/or recycling. The enrichment of Zr in the siliciclastic sediments of Sibuti Formation can be interpreted as the result of recycling processes (Fig. 7). The Zr/Hf ratio values range from 19.7 to 41.4, which are comparable with the values reported for zircon minerals ( $\sim 35\text{--}41$ ; Murali et al. 1983).

#### Provenance

Geochemical data of clastic sediments were mainly used to determine the provenance. The ratio of  $Al_2O_3/TiO_2$  in clastic sediments was generally used to predict the source rock composition. The Al in igneous rocks resides mostly in feldspars

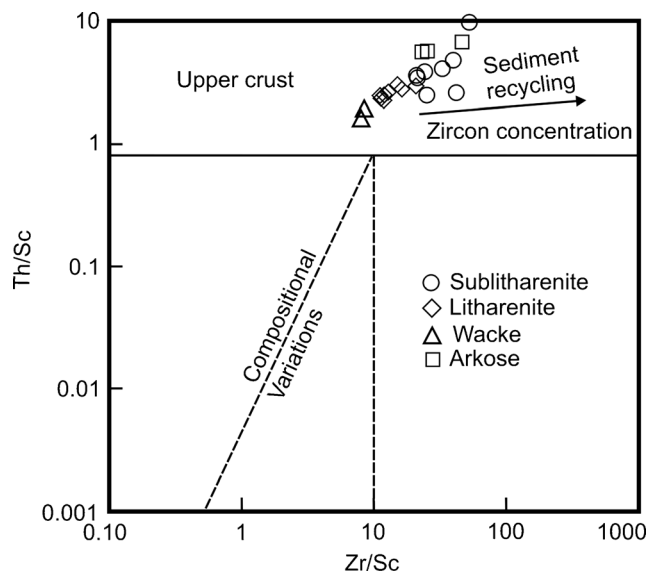


**Fig. 7** Th/Sc versus Zr/Sc diagram for the Sibuti sandstones (after McLennan et al. 1993). The addition of zircon due to sediment sorting and recycling is observed in trend 2

and Ti in mafic minerals (e.g., olivine, pyroxene, hornblende, biotite, ilmenite), and the  $Al_2O_3/TiO_2$  ratios increase from 3 to 8 in mafic igneous rocks, from 8 to 21 in intermediate igneous rocks, and from 21 to 70 in felsic igneous rocks (Hayashi et al. 1997). In general, the variation in the  $Al_2O_3/TiO_2$  ratio (~17.1–24.3) suggests that the samples were derived from intermediate to felsic source rocks. However, one quartz arenite sample (SL3) shows very low average  $Al_2O_3/TiO_2$  ratio (4.67), which may be due to the high sediment maturity and/or presence of significant amount of  $TiO_2$ -rich minerals (ilmenite, anatase, brookite, and rutile).

REE such as Th and Sc are highly useful for provenance study, since these elements are immobile during weathering and are believed to be transported specifically on terrigenous component of sediments, which reflects the chemistry of the source rocks (Cullers 2000). The Sibuti siliciclastic sediments clustered on continental sources field in the Th versus Sc plot (Fig. 8a). Similarly, on the Th/Sc versus Sc plot (Fig. 8b), the samples are clustered above the average UCC and PAAS values and are comparable with average granite composition

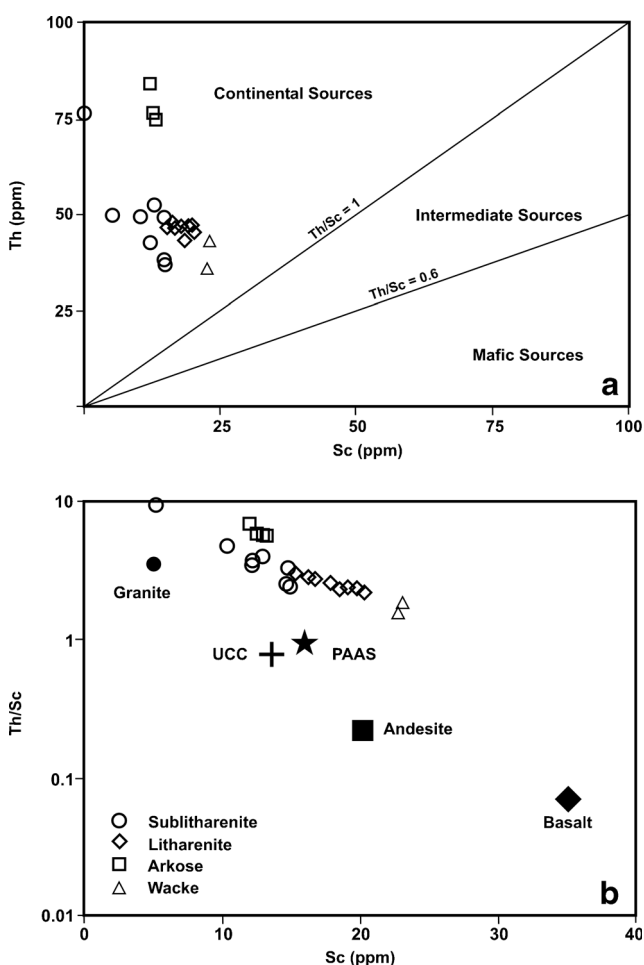


**Fig. 8** Bivariate plot of **a** La versus Sc and **b** Th/Sc versus Sc for Sibuti sandstones

and demonstrates that the sediments were derived from silica-rich continental sources.

Compared to UCC, Cr concentration in felsic rocks is lower than in the intermediate rocks. A higher concentration of Cr (usually 2–10 times) in sedimentary rocks would be a source contribution from mafic to ultramafic rocks. The low concentration of Cr (<150 ppm), Ni (<100 ppm), and Cr/Ni ratio between 1.1 and 3.2 but mostly <2 indicates the absence of widespread mafic/ultramafic rocks in the source region (Armstrong-Altrin et al. 2014). The occurrence of detrital chrome spinel within the quartz arenites probably elevated the Cr concentration up to 205 ppm.

Trace element ratios such as Th/Sc, La/Sc, Th/Sc, Zr/Sc, La/Co, Th/Co, and Cr/Th are sensitive provenance indicators, and differences in mafic/felsic sources would provide information about the provenance of sedimentary rocks (e.g., Cullers 2000; Nagarajan et al. 2007b; Bakkiaraj et al. 2010; Armstrong-Altrin et al. 2012). Geochemical ratios such as La/Sc, Th/Sc, Th/Cr, Cr/Th, La/Co, and Th/Co of the studied samples were compared with probable source rocks (granite, tonalite-trongimite-granite (TTG), felsic volcanic, and andesite), range of sediments from felsic and mafic sources, UCC, and PAAS, which clearly indicates that the studied Sibuti sediments are comparable with the sediments derived from felsic volcanic rocks and granites (Table 2). However, Cr/Th ratios of the studied sediments are comparable with TTG than granite, which may be due to the effect of sorting of sediments during transportation.

Several classification schemes based on major elements have been proposed to understand the provenance and tectonic setting of the clastic sediments. The discrimination diagram based on major elements proposed by Roser and Korsch (1988) with four provenance groups (P1 first-cycle basaltic and minor andesitic detritus, P2 dominantly andesitic materials, P3 acid plutonic and volcanic detritus, and P4 mature polycyclic quartzose detritus) is used to distinguish the provenance of the studied sediments. The provenance diagram (Fig. 9) suggests that the sediments of the Sibuti Formation should be derived from the recycled sources represented by quartzose sediments of mature continental provenance and/or granitic-gneissic source categorized by Roser and Korsch (1988). Two samples each fall in P2 and P1 fields indicating intermediate to mafic composition components in the source region. van Hattum et al. (2006) stated that during early Miocene, effective erosion from Borneo highlands derived a lot of recycled sediments to the deep Cenozoic basins around Borneo and continued steadily throughout the Neogene.

#### Tectonic setting

Major and trace element concentrations of sedimentary rocks can be used to identify the tectonic setting of the source area (Bhatia 1983; Armstrong-Altrin and Verma 2005). Verma and

**Table 2** Range of elemental ratios of clastic sediments of the Sibuti Formation compared to the ratios in similar fractions derived from felsic rocks, mafic rocks, upper continental crust (UCC), and post-Archaean Australian shale (PAAS)

Elemental Ratio	Sediments from Sibuti Formation <sup>a</sup>					Granite <sup>c</sup>	TTG <sup>c</sup>	Felsic volcanic rock <sup>c</sup>	Andesite <sup>e</sup>	Range of sediments <sup>b</sup>		UCC <sup>d</sup>	PAAS <sup>d</sup>
	Arenite (n=3)	Litharenite (n=8)	Sublitharenite (excluding sample SL25) (n=9)	Arkose (n=3)	Wacke (n=2)					Felsic rock	Mafic rock		
La/Sc	–	8.0–11.9	7.6–38.5	16.7–24.1	5.5–7.6	8	1.79	2.8	0.9	2.50–16.3	0.43–0.86	2.21	2.40
Th/Sc	–	2.3–3.1	2.5–9.7	5.7–7.0	1.6–1.9	3.6	0.71	0.9	0.22	0.84–20.5	0.05–0.22	0.79	0.90
Th/Cr	0.5–2.9	0.4–0.5	0.5–1.1	0.8–1.0	0.3–0.4	2.25	0.30	1.5	0.10	0.13–2.7	0.018–0.046	0.13	0.13
Cr/Th	0.4–2.0	2.0–2.4	0.9–2.1	1.0–1.3	2.8–3.2	0.44	3.3	0.67	9.77	4.00–15.0	25–500	7.76	7.53
La/Co	–	6.7–9.8	7.5–120.5	–	4.3–6.6	13.33	1.79	5.6	0.9	1.80–13.8	0.14–0.38	1.76	1.66
Th/Co	–	1.8–2.5	2.5–30.3	–	1.2–1.6	6	0.71	1.8	0.22	0.67–19.4	0.04–1.40	0.63	0.63

<sup>a</sup>This study

<sup>b</sup>Condie (1993)

<sup>c</sup>Cullers (1994, 2000); Cullers and Podkovyrov (2000); Cullers et al. (1988)

<sup>d</sup>Taylor and McLennan (1985); McLennan (2001)

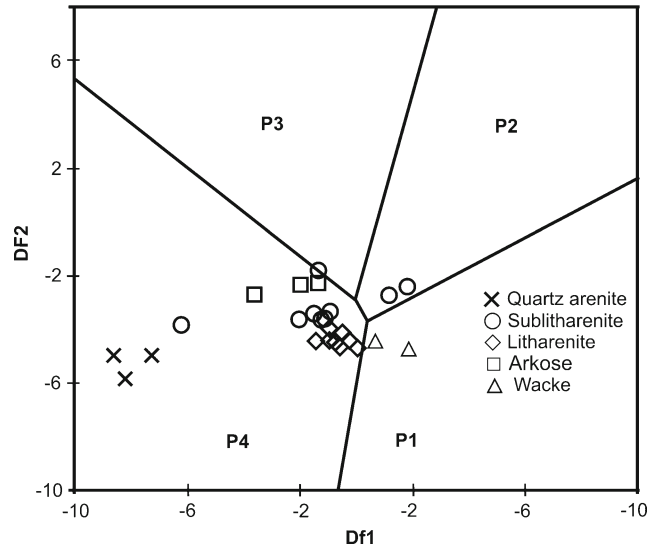


**Fig. 9** Major element provenance discriminant-function diagram for the clastic sediments of the Sibuti Formation (Roser and Korsch 1988). The discriminant functions are the following: discriminant function 1 =  $(-1.773 \cdot \text{TiO}_2) + (0.607 \cdot \text{Al}_2\text{O}_3) + (0.760 \cdot \text{Fe}_2\text{O}_3) + (-1.500 \cdot \text{MgO}) + (0.616 \cdot \text{CaO}) + (0.509 \cdot \text{Na}_2\text{O}) + (-1.224 \cdot \text{K}_2\text{O}) + (-9.090)$ ; discriminant function 2 =  $(0.445 \cdot \text{TiO}_2) + (0.070 \cdot \text{Al}_2\text{O}_3) + (-0.250 \cdot \text{Fe}_2\text{O}_3) + (-1.142 \cdot \text{MgO}) + (0.438 \cdot \text{CaO}) + (1.475 \cdot \text{Na}_2\text{O}) + (-1.426 \cdot \text{K}_2\text{O}) + (-6.861)$ . (P1 first-cycle basaltic and minor andesitic detritus, P2 dominantly andesitic materials, P3 acid plutonic and volcanic detritus, and P4 mature polycyclic quartzose detritus)

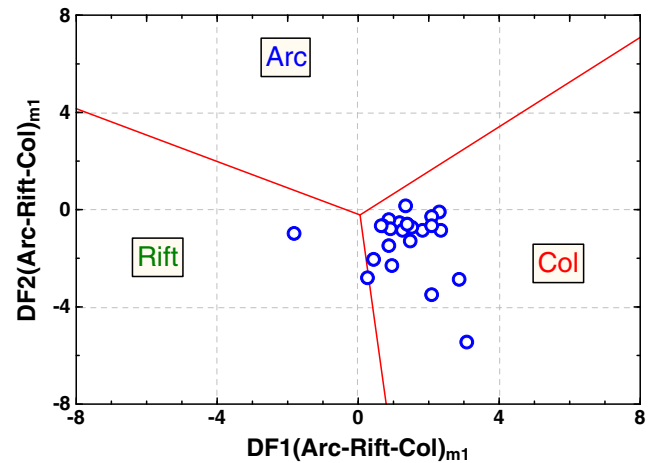


**Fig. 10** Discriminant-function multi-dimensional diagram for high-silica clastic sediments (Verma and Armstrong-Altrin 2013). The subscript  $m_1$  in DF1 and DF2 represents the high-silica diagram based on  $\log_e$ -ratios of major elements. The discriminant-function equations are the following:  $\text{DF1}_{(\text{Arc-Rift-Col})m_1} = (-0.263 \times \ln(\text{TiO}_2/\text{SiO}_2)_{\text{adj}}) + (0.604 \times \ln(\text{Al}_2\text{O}_3/\text{SiO}_2)_{\text{adj}}) + (-1.725 \times \ln(\text{Fe}_2\text{O}_3/\text{SiO}_2)_{\text{adj}}) + (0.660 \times \ln(\text{MnO}/\text{SiO}_2)_{\text{adj}}) + (2.191 \times \ln(\text{MgO}/\text{SiO}_2)_{\text{adj}}) + (0.144 \times \ln(\text{CaO}/\text{SiO}_2)_{\text{adj}}) + (-1.304 \times \ln(\text{Na}_2\text{O}/\text{SiO}_2)_{\text{adj}}) + (0.054 \times \ln(\text{K}_2\text{O}/\text{SiO}_2)_{\text{adj}}) + (-0.330 \times \ln(\text{P}_2\text{O}_5/\text{SiO}_2)_{\text{adj}}) + 1.588$ ;  $\text{DF2}_{(\text{Arc-Rift-Col})m_1} = (-1.196 \times \ln(\text{TiO}_2/\text{SiO}_2)_{\text{adj}}) + (1.604 \times \ln(\text{Al}_2\text{O}_3/\text{SiO}_2)_{\text{adj}}) + (0.303 \times \ln(\text{Fe}_2\text{O}_3/\text{SiO}_2)_{\text{adj}}) + (0.436 \times \ln(\text{MnO}/\text{SiO}_2)_{\text{adj}}) + (0.838 \times \ln(\text{MgO}/\text{SiO}_2)_{\text{adj}}) + (-0.407 \times \ln(\text{CaO}/\text{SiO}_2)_{\text{adj}}) + (1.021 \times \ln(\text{Na}_2\text{O}/\text{SiO}_2)_{\text{adj}}) + (-1.706 \times \ln(\text{K}_2\text{O}/\text{SiO}_2)_{\text{adj}}) + (-0.126 \times \ln(\text{P}_2\text{O}_5/\text{SiO}_2)_{\text{adj}}) - 1.068$

Armstrong-Altrin (2013) proposed two discriminant-function-based major element diagrams for the tectonic discrimination of siliciclastic sediments from three main tectonic settings: Island or continental arc, continental rift, and collision have been created for the tectonic discrimination of high-silica  $[(\text{SiO}_2)_{\text{adj}}=63\text{--}95\ \%]$  and low-silica rocks  $[(\text{SiO}_2)_{\text{adj}}=35\text{--}63\ \%]$ . These two new diagrams were constructed based on worldwide examples of Neogene-Quaternary siliciclastic sediments from known tectonic settings,  $\log_e$ -ratio transformation of ten major elements with  $\text{SiO}_2$  as the common denominator, and linear discriminant analysis of the  $\log_e$ -transformed ratio data. These multi-dimensional diagrams are efficient to provide tectonic discrimination of arc, continental rift, and collision. Recently, these diagrams were evaluated by Armstrong-Altrin (2014) and identified a good functioning of these diagrams for discriminating the tectonic setting of older sedimentary basins. Similarly, these diagrams were used in recent studies to discriminate the tectonic setting of a source region, based on sediment geochemistry (e.g., Zaid and Gahtani 2014). The  $\text{SiO}_2$  content of the Sibuti Formation clastic sediments is  $>63$ ; the high silica diagram of Verma and Armstrong-Altrin (2013) is used to identify the probable tectonic setting of the source area. On this diagram, samples plot mostly in the collision field, except few samples, which plot in the rift field. This result gives an idea that the Sibuti sediments were derived from a passive to moderately active continental collision zone (Fig. 10). These findings were compared with available sources that provided an overview of the study area. During Paleocene to Eocene, there was a regional tectonically active subduction along the Lupar formation toward the central of Kalimantan. This phenomenon was caused by the collision between Luconia and Kalimantan blocks, forming accretionary prism. During the late Eocene, collision of Luconia continental block against northwest Borneo block caused multiple tectonic deformations such as folding, thrusting, and regional upliftment which was termed as Sarawak Orogeny by Hutchison (1996). The Sibuti Formation particularly the sandy layers may be the product of sediment recycling; originating from the exhumation of the Rajang and Croker Mountains that started to raise from the Early Miocene onwards, these provided a limited amount of sand to the shallow Sibuti lagoons. Later, during the Neogene, the total amount of exhumation could have reached 6 km, estimated from the widespread presence of authigenic quartz in basal Rajang group sediments. Mass balancing the Tertiary sediment fill of the NW Borneo deep against erosion within the known river drainage areas although indicates an erosion of 6–7 km in the latter (unpublished). The amount of recycled Tertiary and older sediments within the Sibutican helps to explain its heterogeneous nature. Thus, it is clear from the geochemistry results that the clastic sediments of the Sibuti formation were deposited in a relatively shallow depositional environment.

## Conclusion

Clastic sediments collected from Sibuti Formation were studied for mineralogy and geochemistry in order to understand the intensity of weathering, provenance, and tectonic setting. The mineralogy and geochemistry results revealed that these sediments were moderate to highly mature, and the CIA and PIA values indicated an intensive weathering in the source region. Mineralogically, the studied clastic sediments are enriched with quartz, mica, illite, kaolinite, chlorite, zeolites with little feldspars, and heavy minerals such as zircon, rutile/ilmenite, and tourmaline. Geochemically, the clastic sediments were classified as quartz arenites, sublitharenites, litharenites, arkoses, and wackes.  $\text{Al}_2\text{O}_3/\text{TiO}_2$  ratios showed that the rocks were derived from intermediate to felsic source rocks. Provenance discrimination plots indicated that these sediments were mostly derived from continental silica-rich rocks particularly sediments recycled from sedimentary or metasedimentary sources. Metasediment-rich source area such as Rajang group was probably the source area for the Sibuti Formation. Discriminant-function multi-dimensional diagram showed that the clastic sediments of the Sibuti Formation were derived from a continental collision zone, which is consistent with the geology of the NW Borneo.

**Acknowledgments** First author (RN) would like to thank his bachelor degree students for their help during field work and sample processing. We thank Carlos Linares-López for SEM-EDS. This study was financially supported by Curtin University Research Performance fund awarded to RN. JSA is grateful to the Director, Instituto de Ciencias del Mar y Limnología, Universidad Nacional Autónoma de México for granted permission for an academic stay at the School of Engineering and Science, Curtin University from 29 July 2013 to 9 August 2013 with institutional fund (project no. 616). Authors are indebted to reviewers and editor for their reviews and suggestions on the manuscript.

## References

- Abou Elmagd K, Wahbi Ali-Bik M, Abayazeed SD (2014) Geology and geochemistry of Kurkur bentonites, southern Egypt: provenance, depositional environment, and compositional implication of Paleocene-Eocene thermal maximum. *Arab J Geosci* 7:899–916
- Armstrong-Altrin JS (2014) Evaluation of two multidimensional discrimination diagrams from beach and deep-sea sediments from the Gulf of Mexico and their application to Precambrian clastic sedimentary rocks. *Int Geol Rev*. doi:10.1080/00206814.2014.936055
- Armstrong-Altrin JS, Verma SP (2005) Critical evaluation of six tectonic setting discrimination diagrams using geochemical data of Neogene sediments from known tectonic setting. *Sediment Geol* 177:115–129
- Armstrong-Altrin JS, Lee YI, Verma SP, Ramasamy S (2004) Geochemistry of sandstones from the upper Miocene Kudankulam formation, Southern India: implications for provenance, weathering, and tectonic setting. *J Sed Res* 74(2):285–297
- Armstrong-Altrin JS, Lee YI, Kasper-Zubillaga JJ, Carranza-Edward A, Garcia D, Eby GN, Balaram V, Cruz-Ortiz NL (2012) Geochemistry

- of beach sands along the western Gulf of Mexico, Mexico: implication for provenance. *Chem Erde-Geochem* 72:345–362
- Armstrong-Altrin JS, Nagarajan R, Madhavaraju J, Rosalez-Hoz L, Lee YI, Balam V, Cruz-Martinez A, Avila-Ramirez G (2013) Geochemistry of Jurassic and upper Cretaceous shales from the Molango Region, Hidalgo, eastern Mexico: implications for source-area weathering, provenance, and tectonic setting. *CR Geosci* 345(4):185–202. doi:10.1016/j.crte.2013.03.004
- Armstrong-Altrin JS, Nagarajan R, Lee YI, Kasper-Zubillaga JJ, Córdoba-Saldaña LP (2014) Geochemistry of sands along the San Nicolás and San Carlos beaches, Gulf of California, Mexico: implication for provenance. *Turk J Earth Sci* 23:533–558
- Armstrong-Altrin JS, Machain-Castillo ML, Rosales-Hoz L, Carranza-Edwards A, Sanchez-Cabeza JA, Ruiz-Fernández AC (2015) Geochemistry of deep sea sediments from the south-western Gulf of Mexico, Mexico: implication for depositional environment. *Cont Shelf Res* 95:15–26
- Bakkiraj D, Nagendra R, Nagarajan R, Armstrong-Altrin JS (2010) Geochemistry of sandstones from the upper cretaceous Sillakkudi formation, Cauvery Basin, southern India: implication for provenance. *J Geol Soc India* 76:453–467. doi:10.1007/s12594-010-0128-3
- Balaguru A, Lukie T (2012) Tectono-stratigraphy and development of the Miocene delta systems on an active margin of northwest Borneo, Malaysia. *Warta Geol* 38(2):127–129
- Banda RM (1998) the geology and planktic foraminiferal biostratigraphy of the NW Borneo Basin Sarawak, Malaysia. Ph.D Thesis, University of Tsukuba, Japan
- Bhatia MR (1983) Plate tectonics and geochemical composition of sandstones. *J Geol* 91:611–627
- Blatt HG, Middleton GV, Murray RC (1980) Origin of sedimentary rocks. Prentice-Hall, New Jersey
- Bock B, McLennan SM, Hanson GN (1998) Geochemistry and provenance of the middle ordovician austin glen member (Normanskill Formation) and the Taconian Orogeny in New England. *Sedimentology* 45:635–655
- Condie KC (1993) Chemical composition and evolution of the upper continental crust: contrasting results from surface samples and shales. *Chem Geol* 104:1–37
- Cox R, Lowe DR (1995) A conceptual review of regional-scale controls on the com-position of clastic sediment and the co-evolution of continental blocks and their sedimentary cover. *J Sediment Res* 65:1–21
- Crook KAW (1974) Lithogenesis and tectonics: the significance of compositional variations in flysch arenites graywackes. In: Dott RH, Shaver RH (eds) Modern and ancient geosynclinal sedimentation. *Soc Econ Paleontol Mineral Spec Pub* 19:304–310
- Cullers RL (1994) The controls on the major and trace element variation of shales, siltstones and sandstones of Pennsylvanian–Permian age from uplifted continental blocks in Colorado to platform sediment in Kansas, USA. *Geochim Cosmochim Acta* 58:4955–4972
- Cullers RL (2000) The geochemistry of shales, siltstones and sandstones of Pennsylvanian-Permian age, Colorado, U.S.A.: implications for provenance and metamorphic studies. *Lithos* 51:305–327
- Cullers RL, Podkovyrov VN (2000) Geochemistry of the Mesoproterozoic Lakhanda shales in southeastern Yakutia, Russia: implications for mineralogical and provenance control, and recycling. *Precambrian Res* 104(1–2):77–93
- Cullers RL, Basu A, Suttner LJ (1988) Geochemical signature of provenance in sand-size material in soils and stream sediments near the Tobacco Root batholith, Montana, USA. *Chem Geol* 70:335–348
- Dabard MP (1990) Lower Brioverian formations (Upper Proterozoic) of the Armorican Massif (France): geodynamic evolution of source areas revealed by sandstone petrography and geochemistry. *Sediment Geol* 69:45–58
- Fedo CM, Nesbitt HW, Young GM (1995) Unraveling the effects of potassium metasomatism in sedimentary rocks and paleosols, with implications for weathering conditions and provenance. *Geology* 23(10):921–924
- Fedo CM, Eriksson K, Krogstad EJ (1996) Geochemistry of shales from the Archean (~3.0 Ga) Buhwa Greenstone Belt, Zimbabwe: implications for provenance and source area weathering. *Geochim Cosmochim Acta* 60:1751–1763
- Govindaraju K (1994) Compilation of working values and descriptions for geostandards. *Geostand Newslett* 18:1–158
- Hall R (2013) Contraction and extension in northern Borneo driven by subduction rollback. *J Asian Earth Sci* 76:399–411. doi:10.1016/j.jseas.2013.04.010
- Hall R, Nichols G J (2002) Cenozoic sedimentation and tectonics in Borneo: climatic influences on orogenesis. In: Jones, S. J. & Frostick, L. (Eds.) *Sediment Flux to Basins: Causes, Controls and Consequences*. *Geol Soc London Spl Pub* 191:5–22
- Hall R, Marco WA, van Hattum MWA, Spakman W (2008) Impact of India-Asia collision on SE Asia: the record in Borneo. *Tectonophysics* 451(1–4):366–389. doi:10.1016/j.tecto.2007.11.058
- Hayashi KI, Fujisawa H, Holland HD, Ohmoto H (1997) Geochemistry of ~1.9Ga sedimentary rocks from northeastern Labrador, Canada. *Geochim Cosmochim Acta* 61(19):4115–4137
- Herron MM (1988) Geochemical classification of terrigenous sands and shales from core or log data. *J Sediment Petrol* 58(5):820–829
- Ho KF (1978) Stratigraphic framework for oil exploration in Sarawak. *Geol Soc Malaysia Bull* 10:1–13
- Hofmann AW (1988) Chemical differentiation of the Earth the relationship between mantle, continental crust, and oceanic crust. *Earth Planet Sci Lett* 90:297–314
- Hurowitz JA, McLennan SM (2005) Geochemistry of cambro-ordovician sedimentary rocks of the northeastern United States: changes in sediment sources at the onset of taconian orogenesis. *J Geol* 113: 571–587
- Hutchison CS (1996) The ‘Rajang accretionary prism’ and ‘Lupar Line’ problem of Borneo. In: Hall R, Blundell DJ (eds) *Tectonic Evolution of Southeast Asia*. *Geol Soc London Spec Pub* 106, pp. 247–261
- Hutchison CS (2005) *Geology of north-west Borneo: Sarawak, Brunei and Sabah*. Elsevier, Amsterdam
- Hutchison CS, Bergman SC, Swauger DA, Graves JE (2000) A Miocene collisional belt in north Borneo: uplift mechanism and isostatic adjustment quantified by thermochronology. *J Geol Soc London* 157: 783–793
- Imchen W, Thong GT, Pongen T (2014) Provenance, tectonic setting and age of the sediments of the Upper Disang Formation in the Phek District, Nagaland. *J Asian Earth Sci* 88:11–27
- Jin Z, Li F, Cao J, Wang S, Yu J (2006) Geochemistry of Daihai Lake sediments, Inner Mongolia, north China: implications for provenance, sedimentary sorting and catchment weathering. *Geomorphology* 80:147–163
- Jorge RCGS, Fernandes P, Rodrigues B, Pereira Z, Oliveira JT (2013) Geochemistry and provenance of the Carboniferous Baixo Alentejo Flysch group, South Portuguese Zone. *Sediment Geol* 284–285: 133–148
- Kessler FL (2009) Observations on sediments and deformation characteristics, Sarawak Foreland, Borneo Island. *Warta Geol* 35(1):1–10
- Kessler FL (2010) The Baram Line in Sarawak: comments on its anatomy, history and implications for potential non-conventional gas deposits. *Warta Geol* 35(3):105–110
- Kessler FL, Nagarajan R (2012) A semi-quantitative assessment of clay content in sedimentary rocks using portable X-ray fluorescence spectrometry. *Int J Earth Sci Eng* 05:363–364
- King RC, Backe G, Morley CK, Hillis RR, Tingay MRP (2010) Balancing deformation in NW Borneo: quantifying plate-scale vs.



- gravitational tectonics in a delta and deepwater fold-thrust belt system. *Mar Petrol Geol* 27:238–246
- Liechti PR, Roe FW, Haile NS (1960) The geology of Sarawak, Brunei and the western part of North Borneo. *British Borneo Geol Surv Bull* 3:1–360
- Mat-Zin IC, Tucker ME (1999) An alternative stratigraphic scheme for the Sarawak Basin. *J Asian Earth Sci* 17:215–232
- McLennan SM (2001) Relationships between the trace element composition of sedimentary rocks and upper continental crust. *Geochem geophys geosys* 2(4):1021. doi:10.1029/2000GC000109
- McLennan SM, Taylor SR (1991) Sedimentary rocks and crustal evolution: tectonic setting and secular trends. *J Geol* 99:1–21
- McLennan SM, Nance WB, Taylor SR (1980) Rare earth element-thorium correlation in sedimentary rocks, and the composition of the continental crust. *Geochim Cosmochim Acta* 44:1833–1839
- McLennan SM, Taylor SR, McCulloch MT, Maynard JB (1990) Geochemical and Nd–Sr isotopic composition of deep-sea turbidites—crustal evolution and plate tectonic associations. *Geochim Cosmochim Acta* 54:2015–2050
- McLennan SM, Hemming S, McDaniel DK, Hanson GN (1993) Geochemical approaches to sedimentation, provenance, and tectonics. *Geol Soc Am Spec Papers* 284:21–40. doi:10.1130/SPE284-p21
- Morley CK, Tingay M, Hillis R, King R (2008) Relationship between structural style, overpressures and modern tress, Baram Delta Province, NW Borneo. *J Geophys Res* 113:B09410. doi:10.1029/2007JB005324
- Mortazavi M, Moussavi-Harami R, Mohboubi A, Nadjafi M (2014) Geochemistry of the Late Jurassic-Early Cretaceous shales (Shurijeh Formation) in the intracontinental Kopet-Dagh Basin, northeastern Iran: implication for provenance, source weathering, and paleoenvironments. *Arab J Geosci* 7:5353–5366
- Moss SJ, Wilson MEJ (1998) Biographic implications of the Tertiary paleogeographic evolution of Sulawesi and Borneo. In: Hall R, Holloway JD (eds) *Biogeography and geological evolution of SE Asia*. Backhuys publishers, The Netherlands, pp 133–163
- Murali AV, Parthasarathy R, Mahadevan TM, Sankar D (1983) Trace element characteristics, REE patterns and partition coefficients of zircons from different geological environments—A case study on Indian zircons. *Geochim Cosmochim Acta* 47:2047–2052
- Nagarajan R, Madhavaraju J, Nagendra R, Armstrong-Altrin JS, Moutte J (2007a) Geochemistry of Neoproterozoic shales of Rabanpalli formation, Bhima Basin, Northern Karnataka, southern India: implications for provenance and paleoredox conditions. *Rev Mex Cienc Geol* 24(2):150–160
- Nagarajan R, Armstrong-Altrin JS, Nagendra R, Madhavaraju J, Moutte J (2007b) Petrography and geochemistry of terrigenous sedimentary rocks in the neoproterozoic rabanpalli formation, bhima basin, southern India: implications for paleoweathering conditions, provenance and source rock composition. *J Geol Soc India* 70(2):297–312
- Nagarajan R, Roy PD, Jonathan MP, Lazano R, Kessler FL, Prasanna MV (2014) Geochemistry of Neogene sedimentary rocks from Borneo Basin, East Malaysia: paleo-weathering, provenance, and tectonic setting. *Chem Erde Geochem* 74(1):139–146
- Nesbitt HW, Young GM (1982) Early proterozoic climates and plate motions inferred from major element chemistry of lutites. *Nature* 299(5885):715–717
- Nesbitt HW, Young GM (1984) Prediction of some weathering trends of plutonic and volcanic rocks based on thermodynamic and kinetic considerations. *Geochim Cosmochim Acta* 48(7):1523–1534
- Nesbitt HW, Fedo CM, Young GM (1997) Quartz and feldspar stability, steady and non-steady-state weathering, and petrogenesis of siliciclastic sands and muds. *J Geol* 105:173–191
- Nyakairu GWA, Koeberl C (2001) Mineralogical and chemical composition and distribution of rare earth elements in clay rich sediments from Central Uganda. *Geochem J* 35:13–28
- Peng LC, Leman Md S, Hassan K, Nasib Md B, Karim R (2004) *Stratigraphic Lexicon of Malaysia*. Geol Soc Malaysia, Kuala Lumpur
- Perri F (2014) Composition, provenance and source weathering of Mesozoic sandstones from Western-Central Mediterranean Alpine Chains. *J African Earth Sci* 91:32–43
- Pettijohn FH, Potter PE, Siever R (1972) *Sand and sandstone*. Springer, New York, p 618
- Puchett H (1972) Barium. In: Wedepohl KH (ed) *Handbook of geochemistry*. Springer, Berlin, pp 5601–5602
- Rahman MJJ, Suzuki S (2007) Geochemistry of sandstones from the Miocene Surma group, Bengal Basin, Bangladesh: implications for provenance, tectonic setting and weathering. *Geochem J* 41:415–428
- Roddaz M, Viers J, Brusset S, Baby P, Boucayrand C, Héral G (2006) Controls on weathering and provenance in the Amazonian foreland basin: insights from major and trace element geochemistry of Neogene Amazonian sediments. *Chem Geol* 226:31–65
- Rollinson HR (1993) *Using geochemical data: evaluation, presentation, interpretation*. Routledge, United Kingdom
- Roser BP, Korsch RJ (1988) Provenance signatures of sandstone–mudstone suites determined using discrimination function analysis of major-element data. *Chem Geol* 67:119–139
- Simmons MD, Bidgood MD, Brenac P, Crevello PD, Lambiash JJ, Morley CK (1999) Microfossil assemblages as proxies for precise palaeoenvironmental determination – an example from Miocene sediments of northwest Borneo. In Jones RW, Simmons MD (eds) *Biostratigraphy in production and Development Geology*. Geol Soc Spl Pub 152, pp 219–242
- Skilbeck CG, Cawood PA (1994) Provenance history of a Carboniferous Gondwana margin forearc basin, New England fold belt, eastern Australia: modal and geochemical constraints. *Sediment Geol* 93:107–133
- Tanean H, Paterson D, Endharto M (1996) Source Provenance interpretation of Kutai basin sandstones and the implication for tectono-stratigraphic evolution of Kalimantan. Indonesian petroleum association, proceedings of the 25th annual convention. Jakarta 1:333–345
- Taylor SR, McLennan SM (1985) *The continental crust: its composition and evolution*. Blackwell, Oxford
- Van der Zee W, Urai JL (2005) Processes of normal fault evolution in a siliciclastic sequence: a case study from Miri, Sarawak, Malaysia. *J Struct Geol* 27:2281–2300
- van Hattum MWA, Hall R, Pickard AL, Nichols GJ (2006) SE Asian sediments not from Asia: provenance and geochronology of North Borneo sandstones. *Geology* 34:589–592
- van Hattum MWA, Hall R, Pickard AL, Nichols GJ (2013) Provenance and geochronology of Cenozoic sandstones of northern Borneo. *J Asian Earth Sci* 76:266–282
- Verma SP, Armstrong-Altrin JS (2013) New multi-dimensional diagrams for tectonic discrimination of siliciclastic sediments and their application to precambrian basins. *Chem Geol* 355:117–133
- Vermeij GJ, Raven JGM (2009) Southeast Asia as the birthplace of unusual traits: the Melongenidae (Gastropoda) of northwest Borneo. *Contrib Zool* 78:113–127
- Wannier M, Lesslar P, Lee C, Raven H, Sorkhabi R, Ibrahim A (2011) Geological excursions around Miri, Sarawak. *Ecomedia Software*, Miri
- Zaid SM, Gahtani FA (2014) Provenance, diagenesis, tectonic setting and geochemistry of Hawkesbury sandstone (Middle Triassic), southern Sydney Basin, Australia. *Turk J Earth Sci* 24:72–98